Nuclear Inst. and Methods in Physics Research, A 1052 (2023) 168287

Contents lists available at ScienceDirect

Nuclear Inst. and Methods in Physics Research, A

journal homepage: www.elsevier.com/locate/nima

Full Length Article

Cherenkov diffraction radiation emissions from single electrons and positrons on a fused silica radiator

Silas Ruhrberg Estevez [a], Tobias Baumgartner [a], Johann Bahl [a], Thomas Lehrach [a], Tobias Thole [a], Benildur Nickel [a], Philipp Loewe [a], Lukas Hildebrandt [a], Cristóvão Beirão da Cruz e Silva [c], Paul Schütze [b], Markus Joos [c,*]

[a] Werner-von-Siemens-Gymnasium, Beskidenstr. 1, 14129 Berlin, Germany
[b] Deutsches Elektronen-Synchrotron DESY, Notkestr. 85, 22607 Hamburg, Germany
[c] CERN, Esplanade des Particules 1, Meyrin, 1217 Geneva, Switzerland

ARTICLE INFO

Keywords:
CERN
DESY
Test beam
Beamline for schools
Cherenkov radiation
ChDR

ABSTRACT

Beam diagnostics are crucial for smooth accelerator operations. Many techniques rely on instrumentation in which the beam properties are significantly affected by the measurement. Novel approaches aim to use Cherenkov Diffraction Radiation (ChDR) for non-invasive diagnostics. Unlike regular Cherenkov Radiation, the charged particles do not have to move inside of the medium, but it is sufficient for them to move in its vicinity as long as they are faster than the speed of light in the medium. Changes to the beam properties due to ChDR measurements are consequently negligible. To examine ChDR emission under different conditions, we placed a fused silica radiator in the DESY II Test Beam. We observed increases in ChDR intensity for electron and positron momenta between 1 GeV c^{-1} and 5 GeV c^{-1}. Additionally, we found a larger photon yield for electrons than positrons for increasing particle momenta. However, the significance of these measurements is strongly limited by the accuracy of the conversion from the measured signal to absolute photon numbers. The results suggest a need for further research into the ChDR generation by electrons and positrons and may find application in the design of future beam diagnostic devices.

1. Introduction

Cherenkov radiation is light produced by charged particles when they pass through an optically transparent medium at speeds exceeding the speed of light in that medium [1]. It was first observed experimentally in 1937 by P. A. Cherenkov [2]. He shared the Nobel Prize in Physics 1958 with I. M. Frank and I. Y. Tamm who developed a theoretical model of the phenomenon [3]. The model was improved by Ginzburg and Frank to show the emission originated from dielectric material regions parallel to the particle motion [4]. The radiation emission has since been calculated using electromagnetic field eigenvalues [5] and Di Francia expansions [6]. More recent work has described ChDR generation in different scenarios [7,8].

In the last few years, the existence of ChDR has been proven experimentally [9]. ChDR can be emitted if an ultrarelativistic charged particle moves in the vicinity of a dielectric medium [10]. The atoms of the medium get polarized by the electric field of the ultrarelativistic charged particle, oscillate, and thereby emit light [11] at a characteristic Cherenkov angle $\cos(\theta) = \frac{1}{\beta n}$, where β is the relativistic factor and n is the refractive index of the material. For fused silica ($n = 1.46$) and ultrarelativistic particles ($\beta \approx 1$) the angle is approximately 46.8° [12].

ChDR is polarized as it arises from fields of charged particles inducing dynamic polarization currents at the air–radiator interface [13]. The angular distribution is determined by the spatial arrangement of the particle and radiator [13]. However, ChDR differs from regular Cherenkov Radiation in that both horizontal and vertical components are measurable as only a fraction of the radiation cone is measured [14]. Differences in radiation between the horizontal and vertical direction, depending on the arrangement of beam and radiator, have been observed [9]. Previous experiments have shown an exponential decay of ChDR intensity for increasing distances from the dielectric radiator which they determined to be in good agreement with predictions from polarization radiation theory [9]. Increased ChDR emission rates for electrons at 5.3 GeV compared to 2.1 GeV have also been observed [14] but to our knowledge no detailed analysis of the effect of particle momentum or energy on ChDR generation has been performed.

ChDR has been proposed to be a method for non-invasive beam diagnostics as the particles do not physically interact with the radiator [14]. Beam position and bunch length monitors exploiting ChDR emission have been trialled successfully [10,15]. In this article we

* Corresponding author.
E-mail address: markus.joos@cern.ch (M. Joos).

https://doi.org/10.1016/j.nima.2023.168287
Received 2 October 2022; Received in revised form 28 February 2023; Accepted 6 April 2023
Available online 11 April 2023

present the results of placing a dielectric radiator in the vicinity of a particle beam at the DESY II Test Beam Facility and measuring the emission rates of photons under different conditions. [1] The Test Beam facility allows measurement of ChDR generated by single particles while previous work has focused on particle bunches [9,14]. We focus on a comparison of the emissions from electrons and positrons in the same setup. To our knowledge this has not been done before as previous experiments were conducted on circular colliders where electrons and positrons travel in opposite directions [14].

2. Methods

2.1. Experimental setup

The DESY II Test Beam Facility offers positron and electron beams with selectable momenta from 1 GeV c^{-1} to 6 GeV c^{-1} [18]. A maximum particle rate of 10×10^3 Hz is reached at around 2 GeV c^{-1} [17]. The Test Beam is generated by double conversion of the DESY II synchrotron beam [18]. Bremsstrahlung is produced from 7 µm carbon primary targets held inside the synchrotron beam. The Bremsstrahlung then creates electron–positron–pairs on a secondary metal target with dimension 45 mm × 60 mm [18]. The particles subsequently pass through a dipole magnet, which allows selection of particle type and momentum. A 10 mm × 20 mm collimator constrains the beam before it traverses the experimental setup.

The experimental setup comprises trigger scintillators, a beam telescope consisting of six silicon pixel detectors [19] that are permanently installed at DESY, a photomultiplier tube (PMT) and a fused silica radiator. A sketch of the arrangement of the components of the experimental setup can be seen in Fig. 1. The beam telescope features a high position resolution, in the order of a few micrometers, and low material budget, which enables the reconstruction of particle tracks at the given momentum range and thus an estimation on the relative particle distance to the radiator. It is used in a configuration with three detector planes each before and behind the radiator. In addition, a pair of scintillators is utilized as input to the trigger system. The PMT (ET enterprises 9813QKB) was operated at 1650 V for all experiments and has a spectral response from 165 nm to 630 nm [20]. This is similar to camera systems with a wavelength of 300 nm–700 nm that have been used previously to detect ChDR [9].

The radiator is positioned partially inside the beam, such that the center of the beam spot is located at the edge of the radiator. Thus, a large portion of particles passes in close proximity of the radiator. Inevitably, a significant fraction of particles also traverses the radiator, leading to emission of non-diffraction Cherenkov radiation. To reduce contamination from ambient light, the PMT and radiator were placed in an aluminum box, painted black on the inside. The box was placed on linear motion stages for an alignment transverse to the beam, while the radiator itself was mounted on a rotation stage for an angular alignment parallel to the beam. Fig. 2 shows the setup inside the box including the radiator with alignment stage and the PMT. Beam windows covered with black tape were added to reduce the material budget while maintaining the blocking of ambient light. The PMT was, optionally, equipped with polarization filters in order to study radiation polarization.

[1] All experiments were conducted by high school students under expert guidance as part of the Beamline for Schools (BL4S) competition 2020. BL4S is a worldwide competition offered by CERN since 2014 that provides high school students with the opportunity to conduct their own experiments at a state-of-the-art particle accelerator [16]. In the years 2019–2021, BL4S was co-organized by DESY and held mostly at their facilities in Hamburg due to the Long Shutdown 2 at CERN [17].

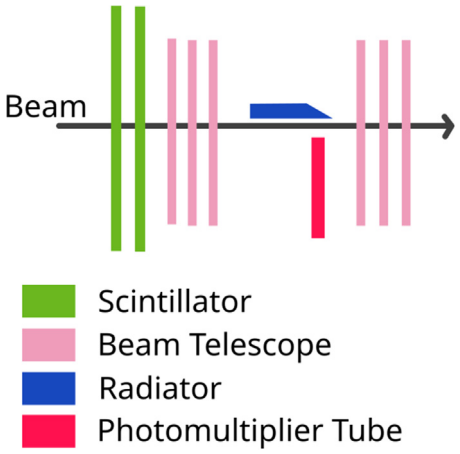

Fig. 1. Sketch of the experimental setup at the DESY II Test beam facility showing the relative positions of the detectors used and the radiator.

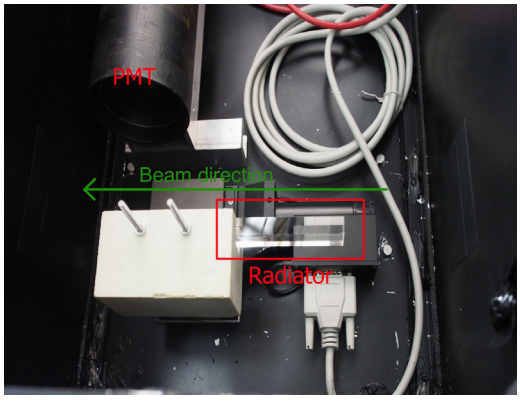

Fig. 2. Picture of the radiator mounted on a rotation stage next to the PMT inside a black painted aluminum box.

2.2. Radiator

Right-angled trapezoid prism radiators made of high purity fused silica (SiO_2) were obtained from Heraeus [21] and CERN. The unique prism geometry of the radiators allows for ChDR generated over the entire length of the radiator to reach the PMT. Fig. 3 shows how light generated along the entire length of the radiator can undergo internal reflections to reach the wedge shaped end of the radiator. A reflective coating at the 21.8° angled surface was applied to enforce the radiation exiting the radiator perpendicularly to the opposite surface. To determine the QDC signal baseline, a small piece of aluminum foil, blocking the light exiting the radiator and entering the PMT, was temporarily applied over this area of the radiator.

2.3. Triggering & data acquisition

Two assemblies of scintillators, light guide and PMT, were used for triggering purposes. These scintillators were powered and their signals interpreted by the Trigger Logic Unit (TLU) [22], which is used for coincidence detection on discriminated input signals with a programmable threshold. The TLU in turn formed a particle trigger signal and performs a trigger-busy-handshake with all detectors, inhibiting any further trigger signals from being distributed while any detector is indicating a busy signal. In consequence of a trigger, the telescope data was recorded, storing the data as well as the trigger numbers to the disk. The PMT signal was digitized via a 12 bit charge to digital converter (QDC) of the type CAEN V965 [23]. For this, an integration

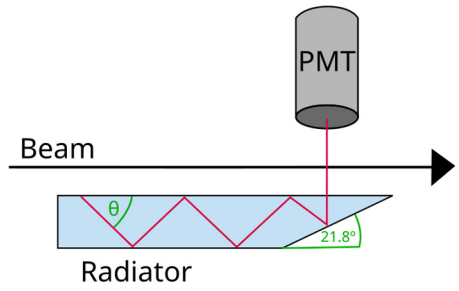

Fig. 3. Sketch of ChDR emission in a long dielectric radiator based on a design previously described for non-invasive beam diagnostics [10].

Table 1
Parameters of the exponential fit of photon emission as a function of impact parameter for different particle types and momenta. The exponential function used was of type $a + b \cdot e^{cx}$.

Beam	a	b	c	χ^2/ndf
1 GeV/c e^-	1.23×10^2	1.69×10^2	0.97×10^1	1.00
1 GeV/c e^+	0.92×10^2	2.04×10^2	1.10×10^1	1.83
2 GeV/c e^-	1.59×10^2	2.39×10^2	1.64×10^1	1.54
2 GeV/c e^+	1.15×10^2	4.51×10^2	1.46×10^1	1.78
3 GeV/c e^-	2.02×10^2	3.33×10^2	1.30×10^1	1.04
3 GeV/c e^+	1.34×10^2	5.66×10^2	1.45×10^1	1.14
4 GeV/c e^-	2.34×10^2	4.95×10^2	1.72×10^1	1.53
4 GeV/c e^+	1.37×10^2	6.76×10^2	1.43×10^1	0.91
5 GeV/c e^-	2.59×10^2	3.86×10^2	1.32×10^1	0.91
5 GeV/c e^+	1.47×10^2	8.95×10^2	1.80×10^1	0.95
6 GeV/c e^+	1.64×10^2	8.62×10^2	1.56×10^1	1.21

window was created through a pulse generator, initiated by the trigger signal and with a width that was empirically determined to cover the full duration of all PMT pulses. The QDC raised a busy signal while the integration is in process. The data acquisition was controlled via the EUDAQ2 data acquisition framework [24]. This software enabled the initialization, configuration and control of the telescope, the QDC, the scintillators, the TLU, and the motion and rotation stages via dedicated configuration files. It furthermore featured so-called data collectors, which have the task of writing the data to disk.

2.4. Data analysis

2.4.1. Determination of radiator boundary

The data was analyzed using ROOT [25] and PyRoot in Jupyter Notebook [26]. The radiator boundary was determined using a Material Budget Image (MBI). The MBI used is a two-dimensional mapping representing the amount of material traversed by relativistic charged particles [27]. The kink angle, the angle between the tracking lines obtained before and after passing through the setup, is used as an estimate of the amount of material the particle traversed [28]. The MBI used is the projection of the kink angle for each particle to a plane within the radiator length approximately halfway between the first and sixth pixel detector of the beam telescope. A difference in the average kink angle between the radiator and the surrounding air can be seen in the MBI in Fig. 4. The boundary of the radiator is defined by the points, in (x, y) coordinates, where the average kink angle is half way between that of air and that of the radiator. The radiator boundary was then estimated by fitting of a straight line through these points, resulting in a close to vertical line. During analysis, the track position at the MBI plane is calculated and the impact parameter is the distance of the track position to the fitted line.

The boundary measurement was performed for each group of runs where the exact position of the radiator could have changed from a previous group of runs, which could happen due to manual interventions on the setup. The standard error of the radiator boundary position was determined from the variance of the (x, y) values compared to the fitted line. On average, the standard error was about 0.02 mm. We decided to use 0.035 mm for the uncertainty of the radiator boundary position from the line fitting as the bin size used in the fit was 0.035 mm. The radiator boundary position was defined for each run as the straight line position subtracted by the value of the standard error.

2.4.2. Analysis of particle tracks

The particle hits were clustered and tracked using the corryvreckan library [29]. The track of the particles in the region of the radiator was calculated by reconstructing the pathway of the particle with straight lines fitted through the clusters before and after the radiator. The particle tracks were used to calculate which particles passed inside the radiator, thus producing non-diffraction Cherenkov radiation, and which particles passed outside the radiator, thus being candidates for producing diffraction Cherenkov radiation. This information is summarized, for each particle, in the impact parameter which is defined as the distance of the track to the radiator surface (as defined in Section 2.4.1), with positive values indicating a position inside the radiator and negative values a position outside the radiator. Events with multiple tracks are removed from analysis. To reduce contamination in the ChDR output from particles that underwent scattering, we have excluded all particles where there is a distance between the predicted values from the upstream and downstream line fitting greater than 0.15 mm, with a distance between a cluster on a single detector and the predicted linear fit greater then 0.2 mm or with an upstream angle greater than 0.005 rad from further analysis.

2.4.3. Comparison of positron and electron beam angular spread

Since the impact parameter is determined at the MBI plane, particles with large impact angles may traverse the radiator at the edges and produce non-diffraction Cherenkov radiation. Analysis of the angular spread in x-direction of the fitted particle tracks for 2 GeV c^{-1} and 5 GeV c^{-1} suggests that there are no significant differences between positrons and electrons (see Fig. 5). The angular spread of the particle tracks decreases as the momentum increases, as expected since the effect of multiple scattering should also decrease.

2.4.4. Analysis of ChDR emission

The average pulse amplitude measured from the PMT was plotted against impact parameter for electrons and positrons respectively (see Figs. 6 and 7). For the initial analysis, the arbitrary QDC output unit values were used as a measure of light intensity. The dotted line in the plot denotes the bias current pedestal, an offset value arising from the QDC measurement process. Events with distances from the radiator boundary greater than 1.2 mm were excluded from the analysis as they were considered to be too far away. The graph obtained was then modeled by an exponential function [9] of type $a + b \cdot e^{cx}$ fitted over 1 mm, ending at a value that corresponds to the uncertainty of the radiator edge (see Figs. 6 and 7). The parameters and χ^2 of the functions for different particle types and momenta are given in Table 1. To obtain a number representative of the total photon production for specific conditions, the fitted function was integrated in the interval. To account for the pedestal, the integral of the pedestal in the same interval was subtracted from this number. Errors of the exponential fit of the data and the subsequent integration were calculated using the ErrorIntegral macro from ROOT [30]. To analyze the contamination from light other than Cherenkov radiation, a run with aluminum foil blocking light generated inside the radiator from entering the PMT was performed and analyzed in the same way (see Fig. 8), no significant contamination was observed and the baseline value (69.52 ± 0.38) is compatible with a pure pedestal background (69.23 ± 0.52). The 6 GeV c^{-1} electron measurement was excluded from the analysis because after tracking there was an insufficient number of data points with accurate tracks (see Fig. 6). However, the experiment with 6 GeV c^{-1} positrons had enough data.

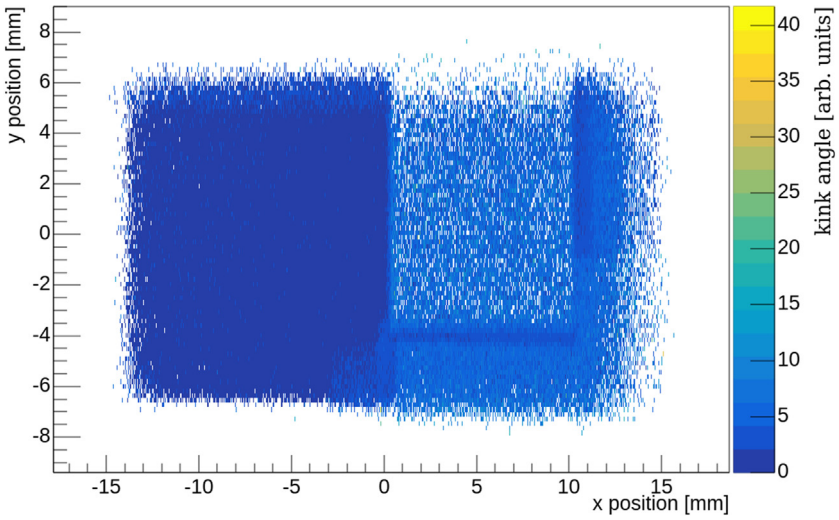

Fig. 4. X–Y projection material budget image of the beam profile kink angle. The left section, in dark blue corresponds to air; the low statistics region with large kink angles, in the top right area, corresponds to the radiator; the region below and to the right of the radiator with slightly increased kink angles compared to the air region, corresponds to the support structure of the radiator; a small gap of air, between the radiator and support structure can also be observed in the darker colors, reflecting a lower kink angle, as expected from the geometric design of the mechanical support; a faint silhouette of a plastic screw and washer from the support structure can also be observed on the bottom, with kink angles between those of air and the support structure itself.

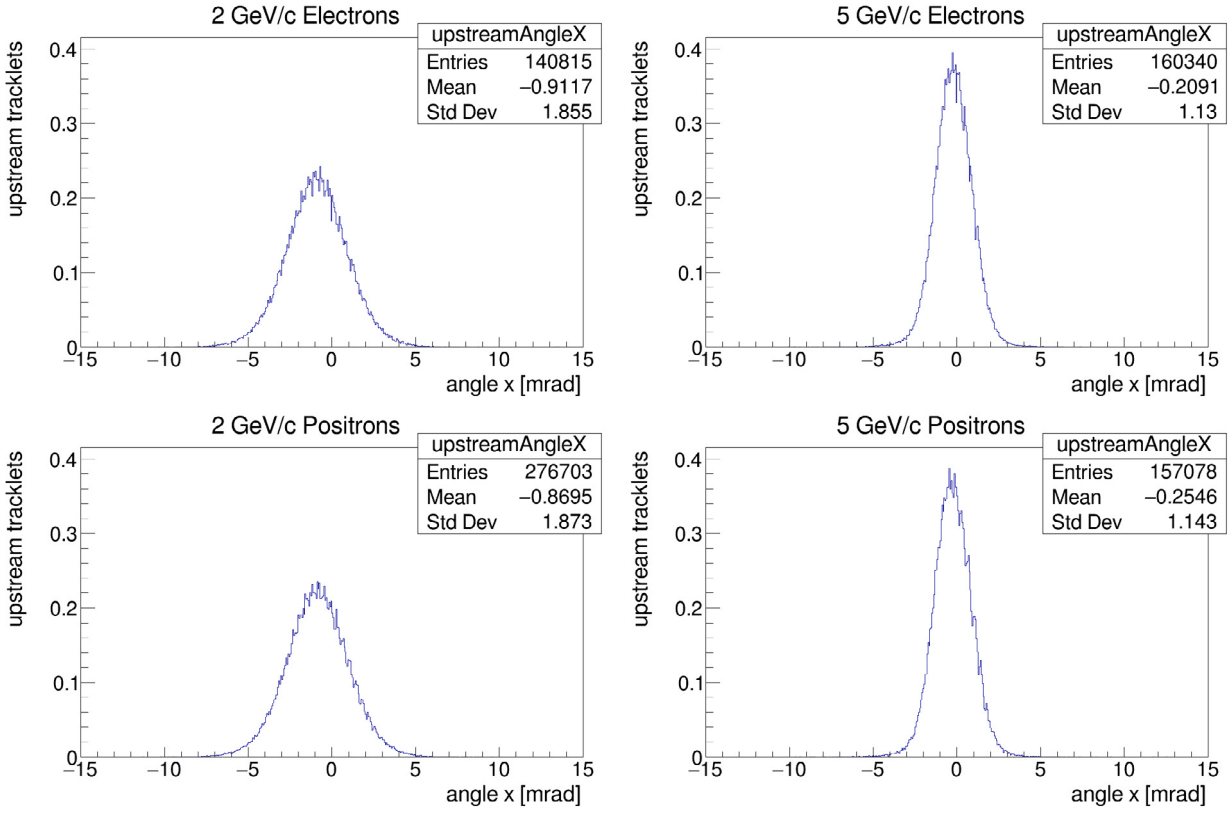

Fig. 5. The distribution of angles of the particle tracks before the radiator for electrons (top) and positrons (bottom) at $2\,\mathrm{GeV\,c^{-1}}$ (left) and $5\,\mathrm{GeV\,c^{-1}}$ (right). No significant differences of the angular spread between electrons and positron beams were observed.

2.4.5. QDC signal calibration

A pulsed green LED in front of the PMT was used to calibrate the QDC output. The distance of the LED as well as current, voltage and duration of the electrical pulses applied to the LED were controlled such that less than 1 in 10 pulses resulted in a signal being produced by the PMT. The number of photons reaching the PMT can be assumed to be a Poisson distribution and in these conditions a Poisson with a mean less than 0.1. Under these circumstances, the probability of having more than one photon is vanishingly small, therefore, the few pulses from the PMT must be from single photon events. By fitting a superposition of two Gaussian functions to the peak in the signal that corresponds to single photons and the bias current pedestal an estimate of the conversion factor from arbitrary QDC units to number of photons can be obtained. Fig. 9 shows the intensity distribution of the QDC output in response to a flashing LED and the Gaussian fits of the data. The measured conversion factor was found to be $(7.48 \pm 3.63)\,\mathrm{QDC units\,photon^{-1}}$. The

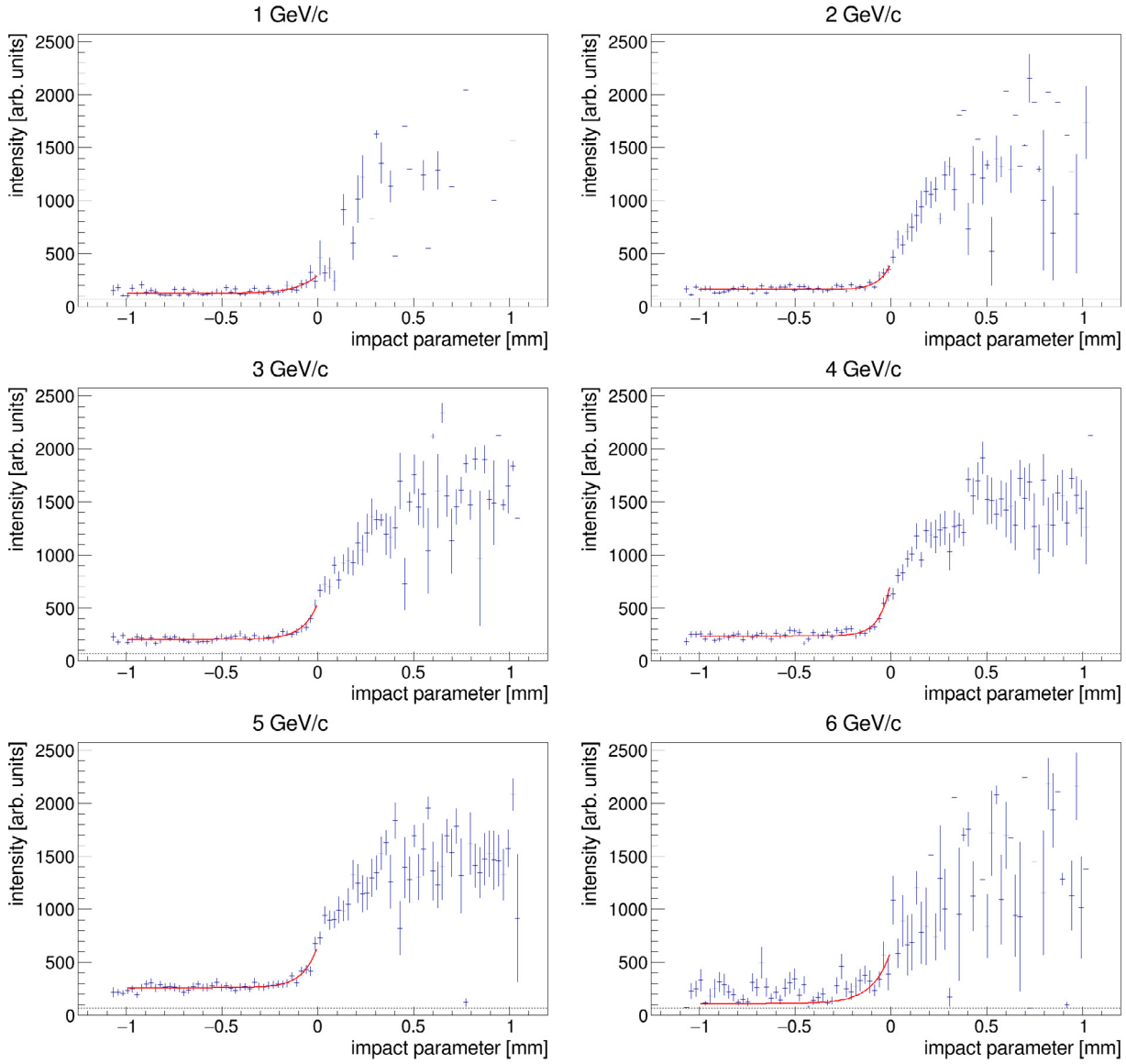

Fig. 6. Histograms of the average light intensity for electrons in arbitrary QDC units as a function of the track impact parameter for beam momenta between $1\,\mathrm{GeV\,c^{-1}}$ and $6\,\mathrm{GeV\,c^{-1}}$. The region immediately outside the radiator is fitted with an exponential.

uncertainty of the conversion factor was calculated using Gauss' law of error propagation and the standard deviations of the individual Gauss functions used in the fitting.

2.4.6. Analysis of total photon emission

Finally, the converted values of the respective integrals were plotted as a function of particle momentum for both electrons and positrons (see Fig. 10). We report the emission of ChDR using the integral of the average amount of photons emitted per particle in the 1 mm interval of interest with the unit [photon mm]. The uncertainty of the photon count was calculated with Gauss' law of error propagation using the uncertainties of the photon conversion and the previously determined error of the integral.

3. Results and discussion

Comparing the experiments with and without aluminum foil suggests a significant increase in photon emission due to Cherenkov Radiation from an interaction between the charged particles and the radiator (see Fig. 8). Application of the foil over the radiator reduced the measured light intensities at all impact parameters to negligible levels. Tracking the particles then allows accurate discrimination between photons generated from non-diffraction Cherenkov Radiation and Cherenkov Diffraction Radiation. We are therefore confident to have detected ChDR. This is supported by our observation of a increase in light emission between $1\,\mathrm{GeV\,c^{-1}}$ and $6\,\mathrm{GeV\,c^{-1}}$ for positrons and $1\,\mathrm{GeV\,c^{-1}}$ and $5\,\mathrm{GeV\,c^{-1}}$ for electrons when comparing the values of the integral of the exponential fit (see Fig. 10). We also observed significantly higher QDC outputs for electrons compared to positrons. However, there is no significant difference in the generation of photons as the QDC units to photon conversion is not very accurate (see Fig. 10). Inside the radiator we observe much higher emissions of light from non-diffraction Cherenkov radiation, although these events are affected by the particle tracking cuts, being removed by the tracking exclusion criteria.

To further characterize the radiation, we measured the photon generation for various orientations of a polarization filter placed over the PMT. The results from this data indicate that ChDR generated in our setup has a higher horizontal than vertical polarization component both at $3\,\mathrm{GeV\,c^{-1}}$ and $5\,\mathrm{GeV\,c^{-1}}$ (see Table 2). Higher emissions of vertically polarized photons for a radiator placed above the beam have been

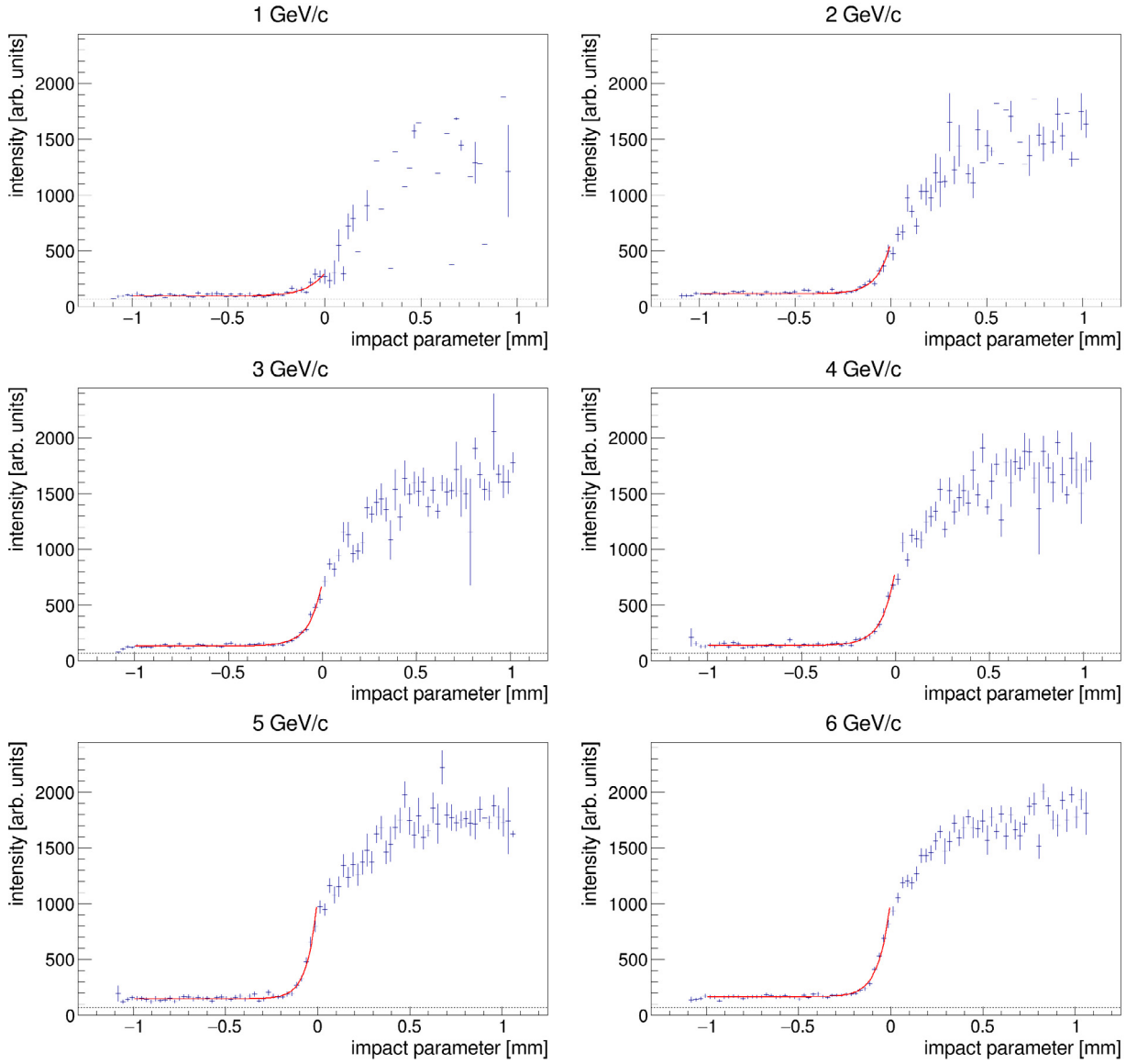

Fig. 7. Histograms of the average light intensity for positrons in arbitrary QDC units as a function of the track impact parameter for beam momenta between $1\,\mathrm{GeV\,c^{-1}}$ and $6\,\mathrm{GeV\,c^{-1}}$. The region immediately outside the radiator is fitted with an exponential.

reported in the literature [14]. As the radiator in our experiment was placed on the side of the beam, our results agree with this observation. The observed light intensity also did not drop to negligible levels when the polarization filter was oriented at 90° to the main polarization direction suggesting both polarization components are present. This seems in agreement with theoretical predictions [14].

We also evaluated a short radiator from CERN on top of the Heraeus radiator we used for the main experiments. The dimensions were $5\,\mathrm{cm}\times 1\,\mathrm{cm}\times 0.5\,\mathrm{cm}$ and $15\,\mathrm{cm}\times 1.5\,\mathrm{cm}\times 1\,\mathrm{cm}$, respectively. The CERN radiator was previously used in other experiments and exhibited some degree of yellowing of the medium, visible by eye, which may affect the light yield of this radiator. Previous experiments suggested a linear increase in light emission for longer radiators [10]. We found an increase in light emission (see Table 3) for the larger radiator, but this was higher than the tripling the theory predicts for a radiator with trice the length [10]. The results of the short radiator also do not support the hypothesis that electrons emit significantly more photons than positrons as there was no significant difference in light emission. The results in the longer radiator may be misleading as the longer radiator could make the setup more sensitive to background Cherenkov radiation produced in air or the black tape input windows. There is also a possibility of photon emission due to ultrarelativistic particles that is not ChDR. This could also explain why we see much higher photon emission in the longer radiator compared to the theoretical prediction. It is however not clear why this would lead to an increase in photon production for electrons compared to positrons. We also show that there are no significant differences between the angular spreads of the respective particle beams, which could have caused increases in light yield, especially for the longer radiator. We also could not verify if there are differences in beam momentum and momentum spread of the DESY Test Beam with the setup used. The deviation from the linear increase in light emission as a function of radiator length is likely due to the yellowing presented by the CERN radiator. Differences in thickness, width or manufacturing of the radiators may also have influenced the measurements.

4. Conclusion

We show that ChDR emission increases with particle momentum between $1\,\mathrm{GeV\,c^{-1}}$ and $5\,\mathrm{GeV\,c^{-1}}$ for both positrons and electrons. Unlike previous experiments on circular colliders, we measured emission by both particle types in the same setup. We report significantly

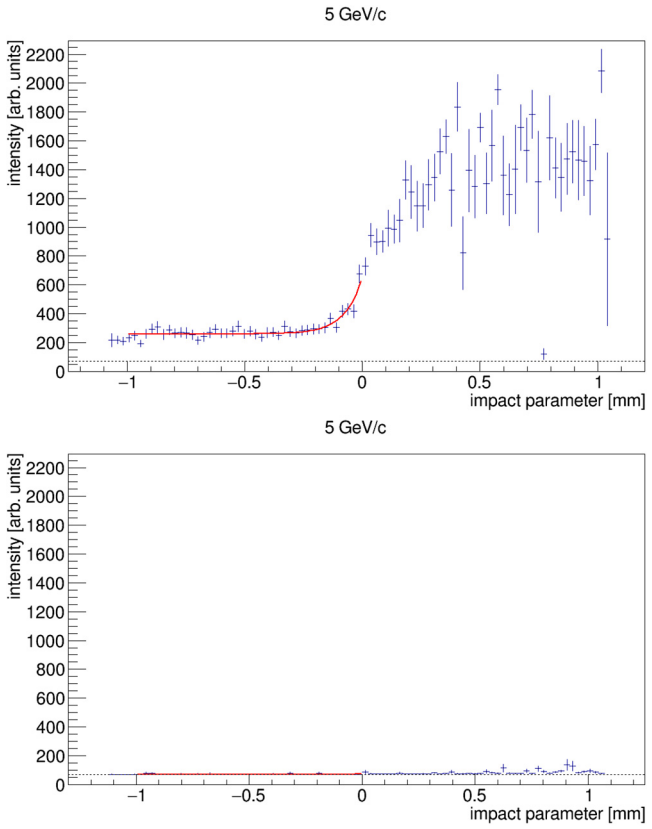

Fig. 8. Histograms of the light intensity in arbitrary QDC units as a function of the track impact parameter for $5\,\mathrm{GeV\,c^{-1}}$ electrons without (top) and with (bottom) an aluminum foil blocking light emission from the radiator. The region immediately outside the radiator is fitted with an exponential. Blocking the photon exit point on the radiator reduces both non-diffraction Cherenkov Radiation and ChDR detection to negligible levels.

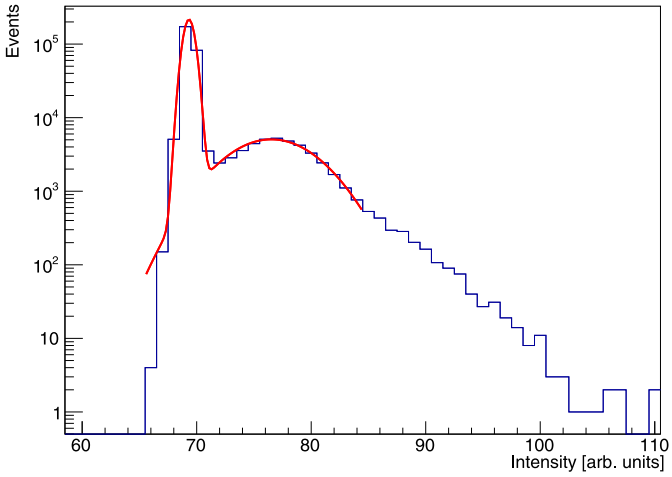

Fig. 9. Measured intensity distribution from a flashing single photon LED (blue line) fitted with a superposition of two Gaussian functions (red line).

higher QDC measurements for electrons compared to positrons between $1\,\mathrm{GeV\,c^{-1}}$ and $5\,\mathrm{GeV\,c^{-1}}$ but this difference is not significant after converting the measurements to photon counts. To our knowledge, differences in emission rates of electrons and positrons have not been reported for ChDR or non-diffraction Cherenkov Radiation. Further experiments to investigate this possible difference are needed because there is uncertainty if the photon conversion in our setup is not accurate enough or there is actually no significant difference. Our results also indicate that ChDR may be useful for monitoring the momenta of particle beams, as the light emissions are a function of the particle momentum for both positrons and electrons.

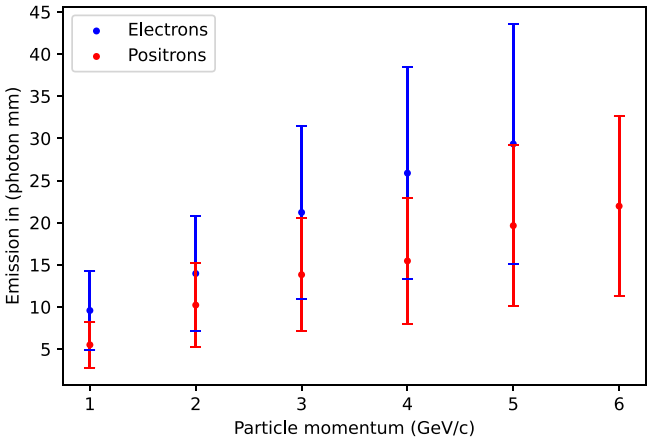

Fig. 10. Values of the converted integral of the exponential fits as a function of beam momentum.

Table 2
Integrated ChDR emissions for $3\,\mathrm{GeV\,c^{-1}}$ and $5\,\mathrm{GeV\,c^{-1}}$ electrons in the 1 mm interval using different orientations of the polarization filters.

Polarization	$3\,\mathrm{GeV\,c^{-1}}$ (photon mm)	$5\,\mathrm{GeV\,c^{-1}}$ (photon mm)
Vertical	0.36 ± 0.17	0.36 ± 0.17
Vertical +45° ccw	0.56 ± 0.27	0.73 ± 0.36
Horizontal	2.10 ± 1.02	2.64 ± 1.28
Horizontal +45° ccw	1.00 ± 0.49	1.28 ± 0.62

Table 3
Integrated ChDR emissions for $2\,\mathrm{GeV\,c^{-1}}$ and $3\,\mathrm{GeV\,c^{-1}}$ electrons and positrons in the 1 mm interval using two different radiators.

Beam	Small radiator (photon mm)	Large radiator (photon mm)
2 GeV e^-	1.02 ± 0.49	13.96 ± 6.78
3 GeV e^-	1.13 ± 0.46	21.21 ± 10.30
2 GeV e^+	0.95 ± 0.54	10.22 ± 4.97
3 GeV e^+	1.19 ± 0.58	13.83 ± 6.71

Declaration of competing interest

The authors declare that they have no known competing financial interests or personal relationships that could have appeared to influence the work reported in this paper.

Data availability

Data will be made available on request.

Acknowledgments

The students among the authors would like to thank their teachers Mr. Seidemann and Mr. Irmer for taking them to CERN and BESSY II and sharing their passion for physics with them. They would also like to thank Sarah Aretz and Margherita Boselli for organizing the competition as well as all volunteers from DESY and CERN for supporting the data analysis. The students are thankful for financial support by the Wilhelm and Else Heraeus Foundation, Germany, the Arconic Foundation, AMGEN, and the Ernest Solvay Fund, managed by the King Baudouin Foundation, that has been provided to BL4S through the CERN and Society Foundation. Receival of radiators from Thibaut

Lefèvre of CERN and Heraeus Group is gratefully acknowledged. The measurements leading to these results have been performed at the Test Beam Facility at DESY Hamburg (Germany), a member of the Helmholtz Association (HGF).

References

[1] Cherenkov radiation, 2022, https://www.britannica.com/science/Cherenkov-radiation. (Accessed 08 September 2022).
[2] P.A. Cherenkov, Visible radiation produced by electrons moving in a medium with velocities exceeding that of light, Phys. Rev. 52 (1937) 378.
[3] I. Tamm, Radiation emitted by uniformly moving particles, J. Phys. 1 (1939) 439–454.
[4] V.L. Ginzburg, I.M. Frank, Radiation of electrons and atoms moving along the axis of a tube in a dense medium, Sov. Phys. Dokl. 56 (1947) 699.
[5] J.G. Linhart, Cherenkov radiation of electrons moving parallel to a dielectric boundary, J. Appl. Phys. 26 (1955) 527, http://dx.doi.org/10.1063/1.1722033.
[6] R. Ulrich, Zur Cherenkov-Strahlung von Elektronen dicht über einem Dielektrikum, Z. Phys. 194 (1966) 180–192, http://dx.doi.org/10.1007/BF01326045.
[7] D. Harryman, et al., Properties of cherenkov diffraction radiation as predicted by the polarisation currents approach for beam instrumentation, 2020, http://dx.doi.org/10.18429/JACoW-IBIC2020-THPP05.
[8] K. Łasocha, et al., Simulation of Cherenkov diffraction radiation for various radiator designs, 2020, http://dx.doi.org/10.18429/JACoW-IBIC2020-TUPP28.
[9] R. Kieffer, et al., Direct observation of incoherent Cherenkov diffraction radiation in the visible range, Phys. Rev. Lett. 121 (2018) 054802, http://dx.doi.org/10.1103/PhysRevLett.121.054802.
[10] D. Alves, et al., Cherenkov diffraction radiation as a tool for beam diagnostics, in: Proceedings of IBIC2019, MalmÖ, Sweden, 2019, http://dx.doi.org/10.18429/JACoW-IBIC2019-THAO01.
[11] L. Bobb, et al., Feasibility of diffraction radiation for noninvasive beam diagnostics as characterized in a storage ring, Phys. Rev. Special Top. Accel. Beams 21 (2018) http://dx.doi.org/10.1103/PhysRevAccelBeams.21.032801.
[12] T. Lefevre, et al., Non-invasive beam diagnostics with Cherenkov diffraction radiation, in: IPAC 2018, JACoW Publishing, 2018, http://dx.doi.org/10.18429/JACoW-IPAC2018-WEPAF074.
[13] M. Shevelev, A. Konkov, Peculiarities of the generation of Vavilov-Cherenkov radiation induced by a charged particle moving past a dielectric target, J. Exp. Theor. Phys. (2014) http://dx.doi.org/10.1134/S1063776114030182.
[14] R. Kieffer, et al., Generation of incoherent Cherenkov diffraction radiation in synchrotrons, Phys. Rev. Accel. Beams 23 (2020) http://dx.doi.org/10.1103/PhysRevAccelBeams.23.042803.
[15] A. Curcio, et al., Noninvasive bunch length measurements exploiting Cherenkov diffraction radiation, Phys. Rev. Accel. Beams 23 (2020) http://dx.doi.org/10.1103/PhysRevAccelBeams.23.022802.
[16] E. Arce-Larreta, et al., Behind the scenes: The two-weeks stay of beamline for schools winning students at DESY, Phys. Educator 03 (2021) 2150001, http://dx.doi.org/10.1142/S2661339521500013.
[17] S. Aretz, et al., An overview of the CERN beamline for schools competition, Phys. Educator 02 (2020) 2050001, http://dx.doi.org/10.1142/S2661339520500018.
[18] R. Diener, et al., The DESY II test beam facility, Nucl. Instrum. Methods Phys. Res. A 922 (2018) http://dx.doi.org/10.1016/j.nima.2018.11.133.
[19] H. Jansen, et al., Performance of the EUDET-type beam telescopes, EPJ Tech. Instrum. 3 (2016) 7, http://dx.doi.org/10.1140/epjti/s40485-016-0033-2.
[20] ET enterprises PMT 9113B series, 2022, https://et-enterprises.com/products/photomultipliers/product/p9813b-series. (Accessed 31 October 2022).
[21] Heraeus, 2022, https://www.heraeus.com/en/group/home/home.html. (Accessed 08 September 2022).
[22] P. Baesso, D. Cussans, J. Goldstein, The AIDA-2020 TLU: a flexible trigger logic unit for test beam facilities, J. Instrum. (2019) http://dx.doi.org/10.1088/1748-0221/14/09/p09019.
[23] CAEN V965, 16 Channel Dual Range Multievent QDC, https://www.caen.it/products/v965/.
[24] Y. Liu, et al., EUDAQ2—A flexible data acquisition software framework for common test beams, J. Instrum. 14 (10) (2019) P10033, http://dx.doi.org/10.1088/1748-0221/14/10/p10033.
[25] ROOT version 6.24.06, CERN, 2022, https://root.cern/ (Accessed 08 September 2022).
[26] Jupyter notebook Python 3.6.8, 2022, https://jupyter.org/, (Accessed 08 September 2022).
[27] H. Jansen, P. Schütze, Feasibility of track-based multiple scattering tomography, Appl. Phys. Lett. 112 (2018) 144101, http://dx.doi.org/10.1063/1.5005503.
[28] M.Q.-M. J. Arling, Radiation length measurements for the ATLAS ITk strip detector, 2022, https://indico.desy.de/event/18050/contributions/28728/attachments/18386/23522/MBI_ATLAS_BTTB6.pdf, (Accessed 31 October 2022).
[29] D. Dannheim, et al., Corryvreckan: a modular 4D track reconstruction and analysis software for test beam data, J. Instrum. 16 (2021) http://dx.doi.org/10.1088/1748-0221/16/03/p03008.
[30] L. Moneta, ErrorIntegral.C file root reference, 2022, https://root.cern/doc/master/ErrorIntegral_8C.html. (Accessed 31 October 2022).